Journal Pre-proofs

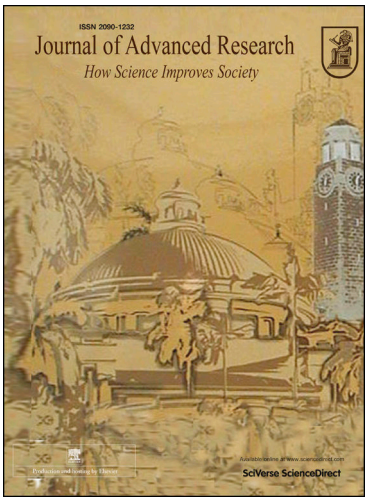

Novel Method to Operation Conditions Identification of High-order Power Converters

Guidong Zhang, Haodong Chen, Samson Shenglong Yu, Zhong Li

PII: S2090-1232(20)30168-5
DOI: https://doi.org/10.1016/j.jare.2020.07.009
Reference: JARE 875

To appear in: *Journal of Advanced Research*

Received Date: 2 June 2020
Accepted Date: 19 July 2020

Please cite this article as: Zhang, G., Chen, H., Yu, S.S., Li, Z., Novel Method to Operation Conditions Identification of High-order Power Converters, *Journal of Advanced Research* (2020), doi: https://doi.org/10.1016/j.jare.2020.07.009

A Novel Approach to Operation Conditions Identification of High-order Power Converters for Reliability Enhancement

Guidong Zhang[a,*], Haodong Chen[a], Samson Shenglong Yu[b], Zhong Li[c]

[a] *Guangdong University of Technology, Guangzhou, 510006, P.R. China;*
[b] *Deakin University, Victoria, Australia;*
[c] *FernUniversität in Hagen, 58084 Hagen, Germany*

Abstract

Intermittent solar energy causes different operational modes of power converters including continuous current modes (CCMs) and discontinuous current modes (DCMs), which need appropriate control strategies and parameters assignment to ensure the functionality of the overall solar energy power generation system. Hence, it is important to identify suitable operation modes for a high-order converter system. However, for a high-order power converter (HOPC), this requires comprehensive analysis and sophisticated control design. This paper focuses on the derivation of operation modes of HOPCs to well identify their boundary conditions. As an example, a 3-Z-network converter is utilized to demonstrate analytical and design process. In detail, the equilibrium points and boundary conditions of each operation modes are first derived; then with the guidance of boundary conditions, unexpected operation modes can be avoided by parameters reassignment. Finally, simulations and experimentation on the newly established system prototype are conducted to validate the effectiveness of the proposed approach.

Keywords: 3-Z-network; boundary condition; modelling and control; parameters assignment and tuning.

*Corresponding author
Email address: guidong.zhang@gdut.edu.cn (Guidong Zhang)

1. Introduction

In the past decades, the renewable energy sector has received substantial investment in infrastructural development. However, for renewable energy integrated energy systems, the technical requirements for power electronics devices have been raised significantly. Firstly, high-ratio boosting techniques with high efficiency and reliability are required to boost low DC voltage generated by renewable energy for grid connection [1–3]. Secondly, effective and efficient modeling and control techniques are needed to compensate for renewable source's intermittency and uncertainty features to realize the system's best working condition [4, 5].

With the advantages of simple structure, high efficiency and high reliability, single-stage high-step-up converters are one of the main methods to realize high voltage conversion ratio [1, 6]. A large quantity of single-stage high-step-up converters combining switched-inductors, switched-capacitors, impedance networks, magnetic coupling devices have been proposed [6–11]. However, few high-step-up converters manage to address and overcome the problems associated with intermittent renewable energy sources, with a majority of them focused on continuous current modes (CCMs) only. With the variation of load, switching frequency and intermittent input voltage, the currents flowing through inductors may reduce to zero and the high-step-up converters will then operate in discontinuous conduction modes (DCMs) [12]. This leads to high input current distortion because of a low gain in CCMs controller, which is inapplicable for DCMs [13, 14]. Moreover, different operation modes produce distinct devices stresses, leading to inapplicability between CCMs and DCMs, electromagnetic interference (EMI) increase and power loss [14–16], which further lead to damage of converters. For better converter design, the boundary conditions of CCMs and DCMs should be well distinguished for power converters connected to renewable sources.

It is noted that power converters are nonlinear systems which are susceptible to factors that may lead to instability [17–20]. A small change of parameters

can lead to bifurcation and deviation from the predefined equilibrium point [21–23]. To find out the operation boundaries of a converter, frequency domain analysis methods can be utilized. However, it requires a large amount of computation [24]. Therefore, another traditional method, i.e., time-domain analysis method based on the average model, has been widely used [25–27]. Furthermore, based on the time-domain analysis method, many modelling methods are proposed, such as circuit averaging and state-space modeling [28–30]. However, it is difficult to build mathematical models for HOPCs. To deal with this issue, a harmonic analysis method was proposed to identify the criteria of different loading conditions to operate at DCMs [31]. However, it bears great inaccuracies and the stability near the switching frequency is unpredicted by time-domain methods. [21]. Compared to time-domain analysis method, boundary conditions for system parameters can be deduced through bifurcation analysis. However, involved mathematical derivations are required and it is difficult to build accurate models [21].

To improve reliability and reduce mathematical complexity, this paper focuses on the operation mode derivation of HOPCs to well identify its boundary conditions and provide industry standards for converter applications. With complex operation modes, 3-Z-network converter proposed in [32] is analysed as a typical example and its derivations of boundary conditions are elaborated.

The remainder of this paper is organized as follows. Section 2 presents four operation modes of 3-Z network converter and gives the equilibrium point of each mode. Based on the derived points, the boundary condition of each mode is illustrated in Section 3. Then, simulation and experimentation are conducted in Sections 4 and 5 to verify the proposed analytical approach for boundary identification. Finally, a conclusion is given in Section 6.

2. An Example: Equilibrium Points Identification for 3-Z-Network Converter

Combined with two switched-inductors, a 3-Z-network converter proposed in [32] is taken as an example in this study and its schematic is shown in Figure 1.

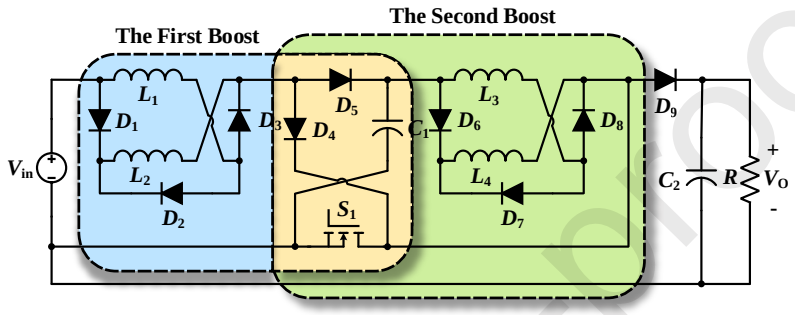

Figure 1: Schematic of the 3-Z-networks boot converter.

Denote $< \cdot >_{T_e}$ as the average value during period $[0,\ T_e]$, where T_e is the switching period. In order to make it easier to understand, $d_1 T_e$ is the period that switch is on; d_2 and d_2' are duty cycles of the two boost stages in DCM, respectively. To simplify the analysis without loss of generality, we impose the following assumptions:

1) All the components are ideal;

2) Filter capacitors C_1 and C_2 are large enough that the voltages across them are constant.

3) $L_1 = L_2 = L_{1,2}$ and $L_3 = L_4 = L_{3,4}$, hence, $i_{L_1} = i_{L_2} = i_{L_{1,2}}$, $i_{L_3} = i_{L_4} = i_{L_{3,4}}$, $v_{L_1} = v_{L_2} = v_{L_{1,2}}$ and $v_{L_3} = v_{L_4} = v_{L_{3,4}}$.

According to the inductor current in each boost stage, four operation modes are briefed as follows, and the waveforms of voltage and current across four inductors are shown in Figure 2. Case I represents that all currents across four inductors are continuous, represented as $C - C$; Case II is that i_{L_1} and i_{L_2} reduce to zero, but i_{L_3} and i_{L_4} are continuous $(C - D)$, while Case III is the opposite case of Case II $(D - C)$; and Case IV represents that i_{L_1}, i_{L_2}, i_{L_3} and

i_{L_4} are all discontinuous $(D-D)$.

Due to the two uncertain duty ratios d_2 and d_2', Case IV $(D-D)$ is the most complicated and its derivation will be deduced as a typical example. As shown in Figure 2 (d), $(d_1+d_2)T_e$ is the instant that the currents across inductors L_1 and L_2 reduce to zero. Moreover, inductors L_3 and L_4 are cut off in the interval $[(d_1+d_2')T_e, T_e]$.

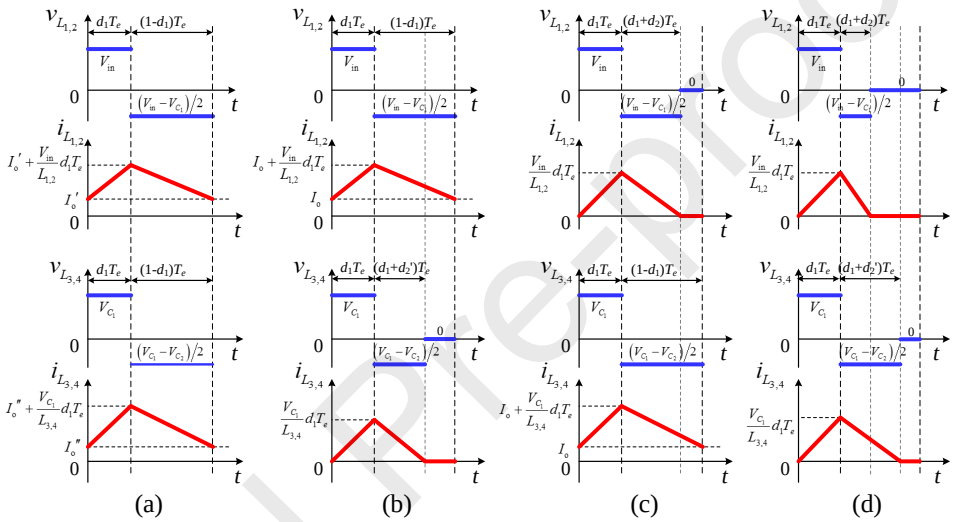

Figure 2: The voltage and current waveforms of L_1, L_2, L_3 and L_4 in each operation mode. (**a**) Case I: $C-C$; (**b**) Case II: $C-D$; (**c**) Case III: $D-C$; (**d**) Case: IV $D-D$.

The average currents through inductors L_1, L_2, L_3 and L_4 can be deduced as

$$I_{L_{1,2}} = \frac{V_{\text{in}}}{2L_{1,2}} d_1 T_e, \tag{1}$$

and

$$I_{L_{3,4}} = \frac{V_{C_1}}{2L_{3,4}} d_1 T_e. \tag{2}$$

In terms of the voltage-second constant theory, we have

$$< v_{L_{1,2}} >_{T_e} = d_1 < v_{\text{in}} >_{T_e} + d_2 \frac{< v_{\text{in}} >_{T_e} - < v_{C_1} >_{T_e}}{2} = 0. \tag{3}$$

Ignoring the impact of ac small signals at the steady state, we have

$$M_1 = \frac{V_{C_1}}{V_{\text{in}}} = \frac{2d_1 + d_2}{d_2}. \tag{4}$$

Similarly, we can obtain the ratio of V_{C_1} and V_{C_2} as

$$M_2 = \frac{V_{C_2}}{V_{C_1}} = \frac{2d_1 + d_2'}{d_2'}, \tag{5}$$

where M_1 and M_2 denote the voltage gains of the first and second boost stages in Figure 1, respectively, and hence, the voltage gain M of the converter is equal to $M_1 \cdot M_2$.

Based on energy conservation, the energy released from L_3 and L_4 during the interval $[d_1T_e, (d_1 + d_2')T_e]$ is equal to the energy dissipation through the load R in a switching period T_e. Hence, one can obtain a quadratic equation as

$$\frac{V_{C_1}}{2L_{3,4}} d_1 T_e V_{C_2} d_2' T_e = \frac{V_{C_2}^2}{R} T_e, \tag{6}$$

i.e.,

$$d_2' = \frac{K_2(1 + \sqrt{1 + 4d_1^2/K_2})}{d_1}, \tag{7}$$

where $K_2 = L_{3,4}/(RT_e)$. Similarly, we can have

$$\frac{V_{\text{in}}}{2L_{1,2}} d_1 T_e V_{C_1} d_2 T_e = \frac{V_{C_2}^2}{R} T_e, \tag{8}$$

which is solved as

$$d_2 = \frac{K_1}{d_1}\left(\frac{2d_1 + d_2'}{d_2'}\right)^2 + \sqrt{\frac{K_1^2}{d_1^2}\left(\frac{2d_1 + d_2'}{d_2'}\right)^4 + 4K_1\left(\frac{2d_1 + d_2'}{d_2'}\right)^2}, \tag{9}$$

where $K_1 = L_{1,2}/(RT_e)$. Therefore, the duties d_2 and d_2', gains M_1 and M_2, and currents are denoted as the functions of d_1, which are listed in Table 1. Similarly with the derivation above, the equilibrium points of Cases I∼III are also listed in Table 1.

3. Boundary Conditions Identification

As shown in Figure 2 (a), the converter is working in Case I $(C - C)$ if and only if $I_{\text{o}}' > 0$ and $I_{\text{o}}'' > 0$ according to the definitions of CCM and DCM. Hence,

Table 1: Equilibrium points of each mode.

Parameter	Case I	Case II	Case III	Case IV
d_2	\	\	$\frac{K_1}{d_1}M_2^2+\sqrt{\frac{K_1^2}{d_1^2}M_2^4+4K_1M_2^2}$	$\frac{K_1}{d_1}M_2^2+\sqrt{\frac{K_1^2}{d_1^2}M_2^4+4K_1M_2^2}$
d_2'	\	$\frac{K_2}{d_1}+\sqrt{\frac{K_2^2}{d_1^2}+4K_2}$	\	$\frac{K_2}{d_1}+\sqrt{\frac{K_2^2}{d_1^2}+4K_2}$
M_1	$\frac{1+d_1}{1-d_1}$	$\frac{1+d_1}{1-d_1}$	$\frac{1}{2}+\frac{1}{2}\sqrt{1+\frac{4d_1^2}{K_1}\cdot M_2^{-2}}$	$1+2\frac{d_1}{d_2}$
M_2	$\frac{1+d_1}{1-d_1}$	$\frac{1}{2}+\frac{1}{2}\sqrt{1+\frac{4d_1^2}{K_2}}$	$\frac{1+d_1}{1-d_1}$	$1+2\frac{d_1}{d_2'}$
$I_{L_{1,2}}$	$\frac{V_{\text{in}}(1+d_1)^3}{R(1-d_1)^4}$	$\frac{2d_1+d_2'}{1-d_1}I_{L_{3,4}}$	$\frac{V_{\text{in}}d_1T_e}{2L_{1,2}}$	$\frac{V_{\text{in}}d_1T_e}{2L_{1,2}}$
$I_{L_{3,4}}$	$\frac{V_{\text{in}}(1+d_1)^2}{R(1-d_1)^3}$	$\frac{M_1V_{\text{in}}d_1T_e}{2L_{3,4}}$	$\frac{d_2}{1+d_1}I_{L_{1,2}}$	$\frac{M_1V_{\text{in}}d_1T_e}{2L_{3,4}}$

average currents $I_{L_{1,2}}$ and $I_{L_{3,4}}$ are larger than half of the current ripple values of $i_{L_{1,2}}$ and $i_{L_{3,4}}$, i.e.,

$$I_{L_{1,2}} > \frac{1}{2}\cdot\frac{V_{\text{in}}d_1T_e}{L_{1,2}}, \tag{10}$$

and

$$I_{L_{3,4}} > \frac{1}{2}\cdot\frac{V_{C_1}d_1T_e}{L_{3,4}}. \tag{11}$$

Substituting $I_{L_{1,2}}$ of Case I in Table 1 into the equations above leads to the existence boundary condition of Case I, as follows,

$$K_{1\_C-C}^{crit}(d_1)=\frac{(1+d_1)^3}{(1-d_1)^4d_1} > \frac{1}{2}\cdot\frac{RT_e}{L_{1,2}}=\frac{1}{2K_1}, \tag{12}$$

and

$$K_{2\_C-C}^{crit}(d_1)=\frac{1+d_1}{(1-d_1)^2d_1} > \frac{1}{2K_2}, \tag{13}$$

where $K_{1\_C-C}^{crit}(d_1)$ and $K_{2\_C-C}^{crit}(d_1)$ are two functions of d_1 corresponding to the first and second boost stages in Case I. Similarly, we can obtain boundary conditions of each operation mode as Table 2.

A numerical example is provided to illustrate the process of mode identification. We assign $R=180\Omega$, $T_e=100\mu s$, $L_{1,2}=0.2mH$, $L_{3,4}=0.7mH$,

Table 2: Boundary conditions of each operating mode

Operating mode	**Boundary Conditions**
Case I	$K^{crit}_{1\_C-C}(d_1) = \frac{(1+d_1)^3}{(1-d_1)^4 d_1} > \frac{1}{2K_1}$
	$K^{crit}_{2\_C-C}(d_1) = \frac{1+d_1}{(1-d_1)^2 d_1} > \frac{1}{2K_2}$
Case II	$K^{crit}_{C-D}(d_1) = \frac{(2d_1+d_2')(1+d_1)}{(1-d_1)^2} > \frac{L_{3,4}}{L_{1,2}}$
	$d_1 + d_2' < 1$
Case III	$K^{crit}_{D-C}(d_1) = \frac{d_2}{(1+d_1)M_1} > \frac{L_{1,2}}{L_{3,4}}$
	$d_1 + d_2 < 1$
Case IV	$d_1 + d_2 < 1$
	$d_1 + d_2' < 1$

$V_{\text{in}} = 10V$ and $d_1 = 0.2$, thus $1/(2K_1) = 45$ and $1/(2K_2) = 12.86$. With Table 1, we can obtain that $K^{crit}_{1\_C-C}(d_1) = 21.09$ and $K^{crit}_{2\_C-C}(d_1) = 9.38$ for Case I; $d_1 + d_2' = 0.83$ and $K^{crit}_{C-D}(d_1) = 1.94$ for Case II; $d_1 + d_2 = 0.67$ and $K^{crit}_{D-C}(d_1) = 0.21$ for Case III; and $d_1 + d_2 = 0.72$ and $d_1 + d_2' = 0.83$ for Case IV. In terms of Table 2, only the condition $d_1 + d_2 < 1, d_1 + d_2' < 1$ of Case IV is valid. Hence, the mode of the converter is determined as Case IV as shown the point A in Figure 3(a).

Parameters d_1 and R vary in practical applications, such as PV systems. In consequence, the operation modes of the converter can be modelled as functions of these two variables. Under the guidance of Table 2, the boundary condition of each mode can be depicted as two or four curves in Figure 3 when $L_{3,4}$ equals $0.7mH$, $0.5mH$ and $0.3mH$. Assuming $d_1 = 0.4$ and $R = 70\Omega$ when $L_{3,4} = 0.5mH$, the converter is in mode Case I as the point A of Figure 3 (b). With the increase of R (from point A to B), the mode transfers from Case I to Case II, and the boundary condition is $d_1 = 0.4$ and $R = 97\Omega$. Similarly, with the decrease of d_1 (from point B to C), the mode transfers from Case II to Case IV, and the boundary condition is $d_1 = 0.27$ and $R = 149\Omega$. In addition,

unexpected modes can be avoided by tuning parameters $L_1 \sim L_4$. For instance, Case III is eliminated in Figure 3 (c) with the decrease of $L_{3,4}$.

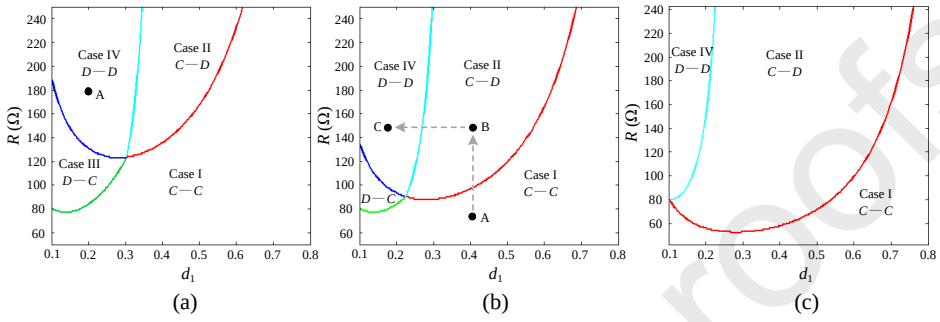

Figure 3: Boundary conditions with varying of $L_{3,4}$ when $T_e = 100\mu s$, $L_{1,2} = 0.2mH$, $V_{\text{in}} = 10V$. (a) $L_{3,4} = 0.7mH$; (b) $L_{3,4} = 0.5mH$; (c) $L_{3,4} = 0.3mH$.

4. Simulation

In this section, MATLAB and Simulink softwares are used to establish the correctness of above mathematical analysis. As listed in Table 7, three sets of component parameters are simulated and obtain validating boundary conditions of Case I and Case II.

Table 3: Parameters of the converter in the simulation.

Parameter	**Value**		
	Set I	**Set II**	**Set III**
Input voltage (V_{in})	10V	2V	2V
Switching period (T_e)	100μs	100μs	100μs
Capacitor (C_1)	1000μF	1000μF	1000μF
Capacitor (C_2)	500μF	500μF	500μF
Inductance (L_1, L_2)	0.2mH	0.2mH	0.2mH
Inductance (L_3, L_4)	0.7mH	0.2mH	0.2mH
Load (R)	$80 \sim 600\Omega$	20Ω	100Ω
Duty (d_1)	0.1~0.6	0.7	0.35

Assume the parameters configured as Set I of Table 7, and the current waveforms of $L_{1,2}$ and $L_{3,4}$ are simulated as shown in Figure 4 when $d_1 = 0.36$, $R = 120\Omega$, $R = 150\Omega$, $R = 180\Omega$, $R = 300\Omega$, $R = 500\Omega$ and $R = 700\Omega$. The minimum of current $I_{L_{3,4}}$ (the solid blue lines) is greater than zero when $R = 120\Omega$, while current $I_{L_{3,4}}$ is obviously discontinuous when $R = 180\Omega$, and the converter is in the critical condition when $R = 150\Omega$. Hence, one of the boundary conditions between $C - C$ and $C - D$ is $d_1 = 0.36$ and $R = 150\Omega$. Similarly, Figure 4 (b) shows another boundary condition between $C - D$ and $D - D$ when $d_1 = 0.36$ and $R = 500\Omega$. With the increasing of d_1 from 0.1 to 0.6, the boundary conditions are measured in the simulation according to the current waveforms of inductors, and the results are plotted in Figure 5 using cross marks. The simulation results are in good agreement with the theoretical results (solid lines in Figure 5).

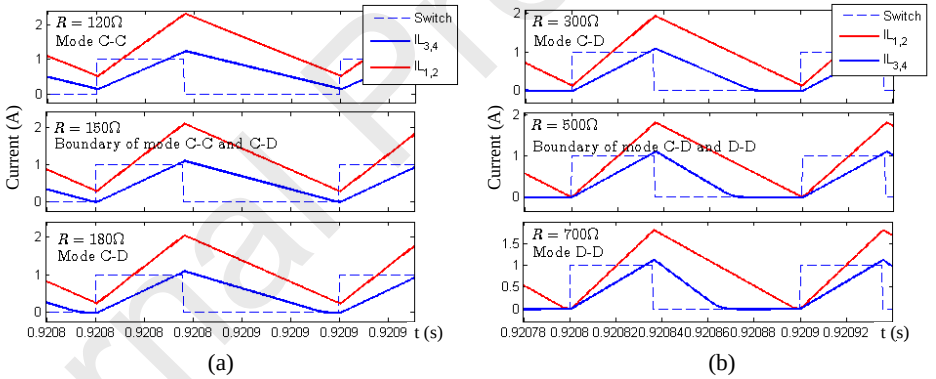

Figure 4: Boundary conditions and current waveforms when $d_1 = 0.36$. (**a**) Boundary condition $d_1 = 0.36$ and $R = 150\Omega$ between $C - C$ and $C - D$; (**b**) Boundary condition $d_1 = 0.36$ and $R = 500\Omega$ between $C - D$ and $D - D$.

5. Experimentation

To verify the correctness of the theoretical analysis, a prototype has been built as shown in Figure 6. The currents flowing through the four inductors

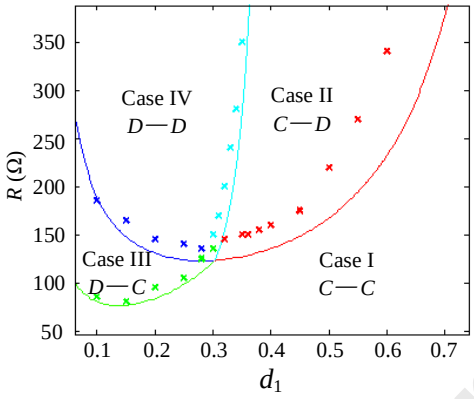

Figure 5: Boundary conditions for d_1 and R in theory and simulation.

can be measured by the current probe, which indicates the operation modes of CCM or DCM.

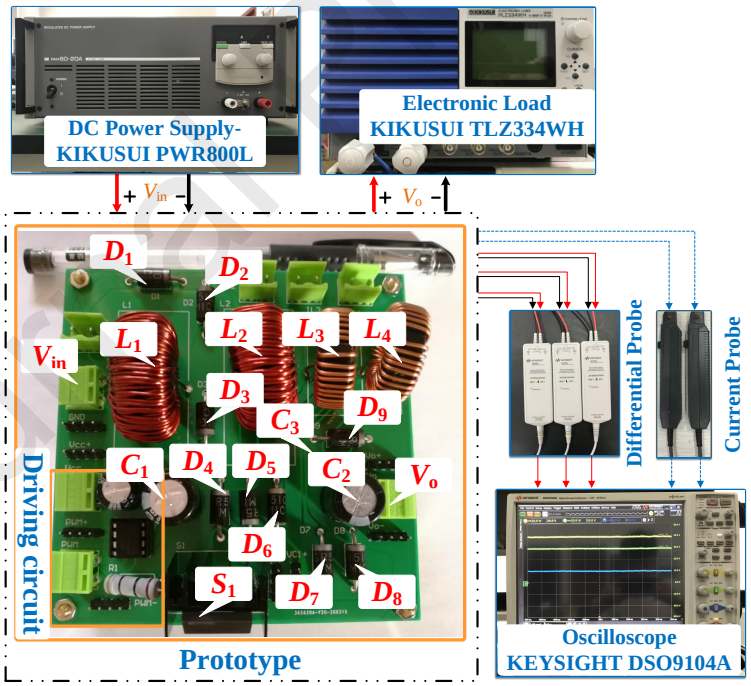

Figure 6: Converter prototype.

According to the derivations mentioned in Section 3, the converter can only operates in Cases I and II with the variation of R and d_1 when $L_{1,2} = 2.75mH$, $L_{3,4} = 0.107mH$, $C_1 = C_2 = 47uF$. The theoretical boundary condition in the $d_1 - R$ 2D coordinate plane is depicted with the blue solid line in Figure 7. In the experiment, the boundary conditions are measured by adjusting the duty cycle d_1 when the load R is fixed at 48.4Ω, 50.1Ω, 54.5Ω, 58.9Ω, 61.5Ω, 67.0Ω, 74.2Ω, 82.3Ω, 92.5Ω, 100.0Ω, 154.0Ω, 202.0Ω and 253.0Ω, respectively for each data point. The results are illustrated by red cross marks in Figure 7. It demonstrates that the theoretical and experimental boundary conditions are in good agreement.

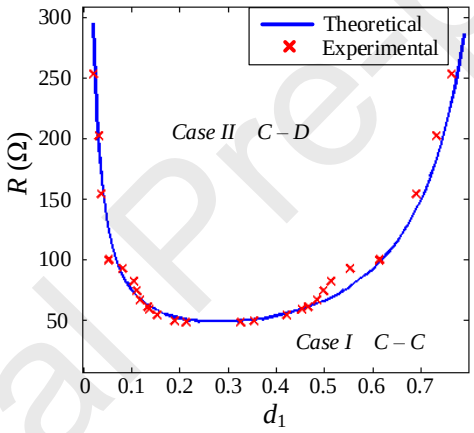

Figure 7: Boundary conditions for d_1 and R in theory and experiments.

6. Conclusion

This paper provides equilibrium points and boundary conditions, and obtains deeper insights into the behaviors of the 3-Z-network converter. The derivations of four operation modes and the boundary condition of each mode has been conducted and provided for the large-signal averaged model of the converter, which provides guidance for engineers to adjust the system parameters so as to realize required operation modes. Simulation and experimentation

have verified the accuracy and effectiveness of the proposed identified operation boundaries.

References

[1] G. Zhang, Z. Li, B. Zhang, W. A. Halang, Power electronics converters: Past, present and future, Renewable and Sustainable Energy Reviews 81 (2018) 2028–2044.

[2] S. Jupin, I. Vechiu, G. Tapia-Otaegui, Universal switched state-space representation for model predictive control of power converters, Electric Power Systems Research 180 (2020) 106120.

[3] D. Ma, W. Chen, L. Shu, X. Qu, X. Zhan, Z. Liu, A multiport power electronic transformer based on modular multilevel converter and mixed-frequency modulation, IEEE Transactions on Circuits and Systems II: Express Briefsdoi:10.1109/TCSII.2019.2931529.

[4] G. Zhang, J. Yuan, Z. Li, S. S. Yu, S.-Z. Chen, H. Trinh, Y. Zhang, Forming a reliable hybrid microgrid using electric spring coupled with non-sensitive loads and ess, IEEE Transactions on Smart Griddoi:10.1109/TSG.2020.2970486.

[5] G. Zhang, J. Yuan, S. Y. Samson, N. Zhang, Y. Wang, Y. Zhang, Advanced four-mode-modulation-based four-switch non-inverting buck–boost converter with extra operation zone, IET Power Electronicsdoi:10.1049/iet-pel.2019.1540.

[6] M. Forouzesh, Y. P. Siwakoti, S. A. Gorji, F. Blaabjerg, B. Lehman, Step-up dc–dc converters: a comprehensive review of voltage-boosting techniques, topologies, and applications, IEEE Transactions on Power Electronics 32 (12) (2017) 9143–9178.

[7] F. Z. Peng, Z-source inverters, Wiley Encyclopedia of Electrical and Electronics Engineering (1999) 1–11.

[8] D. Li, P. C. Loh, M. Zhu, F. Gao, F. Blaabjerg, Generalized multicell switched-inductor and switched-capacitor z-source inverters, IEEE Transactions on Power Electronics 28 (2) (2012) 837–848.

[9] G. Zhang, Z. Wang, H. H.-C. Iu, S.-Z. Chen, Y. Ye, B. Zhang, Y. Zhang, Unique modular structure of multicell high-boost converters with reduced component currents, IEEE Transactions on Power Electronics 33 (9) (2017) 7795–7804.

[10] B. Zhu, F. Ding, D. M. Vilathgamuwa, Coat circuits for dc–dc converters to improve voltage conversion ratio, IEEE Transactions on Power Electronics 35 (4) (2019) 3679–3687.

[11] L. Zhao, J. Chen, T. Chen, Y. Shi, Z. Fan, Z. Zhuang, Zero-voltage and zero-current-switching dual-transformer-based full-bridge converter with current doubler rectifier, IEEE Transactions on Power Electronicsdoi:10.1109/TPEL.2020.2997017.

[12] S. Dong, Q. Zhang, Ccm and dcm analysis of asc-qzsis, IET Power Electronics 12 (8) (2019) 2049–2057.

[13] S. F. Lim, A. M. Khambadkone, A simple digital dcm control scheme for boost pfc operating in both ccm and dcm, IEEE Transactions on Industry Applications 47 (4) (2011) 1802–1812.

[14] K. De Gusseme, D. M. Van de Sype, A. P. Van den Bossche, J. A. Melkebeek, Input-current distortion of ccm boost pfc converters operated in dcm, IEEE Transactions on Industrial Electronics 54 (2) (2007) 858–865.

[15] R. Min, Q. Tong, Q. Zhang, X. Zou, K. Yu, Z. Liu, Digital sensorless current mode control based on charge balance principle and dual current error compensation for dc–dc converters in dcm, IEEE Transactions on Industrial Electronics 63 (1) (2015) 155–166.

[16] D.-H. Kim, G.-Y. Choe, B.-K. Lee, Dcm analysis and inductance design method of interleaved boost converters, IEEE transactions on power electronics 28 (10) (2013) 4700–4711.

[17] D. C. Hamill, J. H. Deane, D. J. Jefferies, Modeling of chaotic dc-dc converters by iterated nonlinear mappings, IEEE transactions on Power Electronics 7 (1) (1992) 25–36.

[18] Y. Chen, K. T. Chi, S.-S. Qiu, L. Lindenmuller, W. Schwarz, Coexisting fast-scale and slow-scale instability in current-mode controlled dc/dc converters: Analysis, simulation and experimental results, IEEE Transactions on Circuits and Systems I: Regular Papers 55 (10) (2008) 3335–3348.

[19] A. El Aroudi, E. Rodríguez, R. Leyva, E. Alarcón, A design-oriented combined approach for bifurcation prediction in switched-mode power converters, IEEE Transactions on Circuits and Systems II: Express Briefs 57 (3) (2010) 218–222.

[20] T. Hu, A nonlinear-system approach to analysis and design of power-electronic converters with saturation and bilinear terms, IEEE Transactions on Power Electronics 26 (2) (2010) 399–410.

[21] X. Xiong, K. T. Chi, X. Ruan, Bifurcation analysis of standalone photovoltaic-battery hybrid power system, IEEE Transactions on Circuits and Systems I: Regular Papers 60 (5) (2013) 1354–1365.

[22] Z. Shuai, Y. Peng, X. Liu, Z. Li, J. M. Guerrero, Z. J. Shen, Parameter stability region analysis of islanded microgrid based on bifurcation theory, IEEE Transactions on Smart Grid 10 (6) (2019) 6580–6591.

[23] D. Dai, C. Tse, X. Ma, Symbolic analysis of switching systems: Application to bifurcation analysis of dc/dc switching converters, IEEE Transactions on Circuits and Systems I: Regular Papers 52 (8) (2005) 1632–1643.

[24] C. Wan, M. Huang, K. T. Chi, X. Ruan, Effects of interaction of power converters coupled via power grid: A design-oriented study, IEEE Transactions on Power Electronics 30 (7) (2014) 3589–3600.

[25] A. Safaee, K. Woronowicz, Time-domain analysis of voltage-driven series–series compensated inductive power transfer topology, IEEE Transactions on Power Electronics 32 (7) (2016) 4981–5003.

[26] H. Li, Z. Guo, C. Liu, T. Q. Zheng, An extensible stability analysis method in time domain for cascaded dc-dc converters in electrical vehicles, Microelectronics Reliability 88 (2018) 1293–1299.

[27] G. Scarciotti, A. Astolfi, Moment-based discontinuous phasor transform and its application to the steady-state analysis of inverters and wireless power transfer systems, IEEE Transactions on Power Electronics 31 (12) (2016) 8448–8460.

[28] Z. Zhang, S. Tian, K. D. Ngo, Small-signal equivalent circuit model of quasi-square-wave flyback converter, IEEE Transactions on Power Electronics 32 (8) (2017) 5885–5888.

[29] G. Bergna-Diaz, J. Freytes, X. Guillaud, S. D'Arco, J. A. Suul, Generalized voltage-based state-space modeling of modular multilevel converters with constant equilibrium in steady state, IEEE Journal of Emerging and Selected Topics in Power Electronics 6 (2) (2018) 707–725.

[30] A. Ayachit, M. K. Kazimierczuk, Averaged small-signal model of pwm dc-dc converters in ccm including switching power loss, IEEE Transactions on Circuits and Systems II: Express Briefs 66 (2) (2018) 262–266.

[31] X. Qu, Y. Jing, J. Lian, S.-C. Wong, K. T. Chi, Design for continuous-current-mode operation of inductive-power-transfer converters with load-independent output, IET Power Electronics 12 (10) (2019) 2458–2465.

[32] G. Zhang, B. Zhang, Z. Li, D. Qiu, L. Yang, W. A. Halang, A 3-Z-network boost converter, IEEE transactions on industrial electronics 62 (1) (2014) 278–288.

Conflict of Interest

The authors have declared no conflict of interest

Corresponding author

Guidong Zhang

Compliance with Ethics Requirements

This article does not contain any studies with human or animal subjects

Corresponding author

Guidong Zhang